JOURNAL OF SPACECRAFT AND ROCKETS
Vol. 32, No. 2, March–April 1995

Leading-Edge Sweepback and Shape Effects on Fin-Induced Fluctuating Pressures

K. Kleifges* and D. S. Dolling†
University of Texas at Austin, Austin, Texas 78712

Measurements of the fluctuating wall pressure have been made on centerline upstream of blunt fins in a Mach 5 turbulent boundary layer. Leading-edge sweep considerably reduces the mean and rms pressure loading at the fin root, the extent of the region of unsteady separation shock motion (i.e., the intermittent region), and the separation length. The frequency of shock-induced pressure fluctuations in the intermittent region increases with leading-edge sweepback, while frequency spectra in the separated region are virtually unchanged. A strake at the root of an unswept fin has virtually no effect, whereas a swept blunted root fillet reduces the upstream influence and intermittent region lengths by 50%, and reduces the mean and rms pressure loading at the fin root by about 75% and 95%, respectively. Experiments using hemicylindrical, wedge-shaped, and flat leading edges show that separated-flow scales and root loading increase with increasing "bluntness" (i.e., wedge to hemicylinder to flat), while the intermittent-region length increases (in terms of fin thicknesses). The changes in flowfield unsteadiness are related to changes in separated-flow structure which alter the dynamics of the primary vortex and recirculation process.

Nomenclature

D	= fin leading-edge diameter
f	= frequency, kHz
f_c	= shock zero-crossing frequency, Eq. (1)
$G(f)$	= power spectral density, psi^2/Hz
$G'(f)$	= $G(f) \cdot f/\sigma^2$
L_i	= intermittent region length
M	= Mach number
N	= number of data points, Eq. (1)
P	= pressure
t	= time, or fin thickness
x	= streamwise distance from fin leading edge
y	= distance vertically above test surface
γ	= shock-foot intermittency, Eq. (1)
λ_{LE}	= sweepback angle of fin leading edge
σ	= rms of pressure fluctuations
τ	= cross-correlation time delay

Subscripts

MAX	= maximum value
w	= value at wall
0	= beginning of interaction
∞	= freestream value

Superscript

—	= mean value

Introduction

Background

EXPERIMENTAL work in transonic,[1,2] supersonic,[3–5] and hypersonic[6] turbulent flows shows that the separated flowfield generated by a hemicylindrically blunted fin or circular cylinder mounted normal to a flat test surface is unsteady. In such flows, separation is intermittent, typically occurring between 2 and 3 diameters (D) upstream of the cylinder or fin leading edge.[7] Motion of the instantaneous separation location is broadband ranging from a few hundred hertz to several kilohertz.[8] The well-defined line seen in surface tracer patterns, called the separation line, is actually the downstream boundary of this region of intermittent separation.[9] The translating separation shock wave generates large-amplitude, low-frequency fluctuating pressure loads in the vicinity of separation. The subsequent expansion and contraction of the separated flow also causes large fluctuating loads, exceeding 180 dB, at the fin root. Analysis of the sparse data base suggests that loading levels increase in intensity with increasing Mach number.[8] Recent work of Shifen and Qingquan[6] shows that the heat transfer is also intermittent and that near separation there is a local rms peak in heating as well as in wall pressure.

Fatigue-life estimates made by Pozefsky et al.[10] for a generic airbreathing transatmospheric vehicle indicate that such loading, combined with high heating, poses a severe threat to local structural integrity. Thus practical methods are needed to control, or at least influence favorably, flowfield unsteadiness. This includes reducing overall load levels, shifting their spectral content away from structural resonant frequencies, and reducing the surface area exposed to high loads. An understanding of the mechanism responsible for the unsteadiness is obviously a prerequisite for success. To date, work has shown that the dominant cause of the shock-foot motion is the displacement due to expansion and contraction of the separated flow.[11–13] This effect raises the question of whether fin geometry changes, which change the separated flow scale or structure, can be used to influence the shock-wave dynamics favorably.

From the work of Price and Stallings[14] in the mid 1960s, the effects of leading-edge sweepback are well documented. Mean wall pressures and shadow photographs over the range $2.3 \leq M_\infty \leq 4.44$, $0 \leq \lambda_{LE} \leq 75$ deg showed that increasing λ_{LE} from 0 to 30 deg sharply decreased the upstream influence, separated-flow scale, and root pressure level. More recently, Hussain[15] obtained wall pressure distributions and surface tracer patterns upstream of hemicylindrically blunted fins for 0 deg $\leq \lambda_{LE} \leq$ 75 deg at a Mach number of 2.4. The angle of attack was varied from 0 to 21 deg. As in Ref. 14, the most dramatic effect of sweep angle occurred between 0 and 30 deg, and it was noted that "while bluntness intensified the interaction, sweep alleviated its intensity." A pertinent observation was that "the multiplicity of the separation and attachment lines on the sidewall and the fin surface, suggested a system of vortices in the interaction region," and that the number of vortices depended on fin leading-edge diameter, sweepback angle, and angle of attack. Sedney[16] has shown that the number of vortices also depends on Mach and Reynolds number. However, since Hussain measured only mean wall pressures, no conclusions could be drawn regarding how the vortices, and the number present, influenced the flowfield un-

Received Oct. 18, 1993; revision received July 14, 1994; accepted for publication July 28, 1994.

*Graduate Student; currently Captain, U.S. Air Force, Phillips Laboratory, Kirtland Air Force Base, NM 87117. Member AIAA.

†Professor, Center for Aeromechanics Research. Associate Fellow AIAA.

steadiness. Based on his work and that of Sedney, the unsteady-flow behavior is likely to be complex. Some very limited observations of flowfield unsteadiness for hemicylindrically blunted swept fins have been made by Blank[17] from schlieren movies with a framing rate of 4 kHz. For a 45-deg swept fin, Ref. 17 noted that "the separation shock is located roughly $0.5t$ upstream of the fin root, and the areas affected by the unsteady separation shock are reduced with respect to the unswept case." A further study using a fillet that was not thicker than the fin produced "significant reduction of flowfield unsteadiness."

Dolling and Rodi[18] examined the effects of leading-edge shape on upstream influence and separated-flow length. The fins were unswept and had hemicylindrical, flat, wedge-shaped, and elliptical leading edges. In studies at Mach 5, it was found that upstream influence increased linearly with wedge angle, from $0.5t$ at 30 deg to $6t$ at 90 deg. It was also shown that the separated-flow length correlated with the fin leading-edge drag coefficient. Thus, fins with a hemicylindrical and with a 53-deg wedge leading edge generate interactions with the same flow scales. Again, only mean wall pressure measurements were made, and thus it is not known how the scale and type of separated flow affects the fluctuating loads. No other experiments are known to the authors in which this question has been addressed, and, as far as is known, no computational methods exist for calculating the flowfield dynamics, although there have been computations of the mean field. Hung and Buning[19] were the first to compute the interaction for an unswept blunt fin and to obtain good comparisons with the experimental results of Dolling and Bogdonoff[20] at Mach 3. More recently, Lakshmanan and Tiwari[21] have used the same code to examine the effects of leading-edge sweepback, and good comparisons were obtained with the experimental results of Ref. 14. Hung[22] also computed the flowfield generated by a flat-faced fin at Mach 5 and obtained good comparisons with the experimental data of Ref. 18.

Thus the literature shows that the scale and structure of the separated flow is dependent on leading-edge geometry and incoming flow conditions, and that computations can capture the essential mean features of the flowfield. A relevant question is whether advantage can be taken of specific configurations to influence the unsteadiness favorably, without significant degradation of component performance. The current experimental investigation was carried out to investigate this question, and will address the following: 1) what are the effects of leading-edge sweepback and leading-edge shape on fluctuating load levels in blunt-fin-induced turbulent interactions; 2) can minor modifications to the configuration of an unswept blunt fin (using fillets or strakes) favorably influence fluctuating load levels; 3) are differences in separated flow structure responsible for any observed differences in flowfield unsteadiness and loading levels?

Experimental Program

Wind-Tunnel and Flow Conditions

All experiments were conducted in the Mach 5 blowdown wind tunnel of the University of Texas at Austin. The test section is 6 in. wide by 7 in. high and is 27 in. long. Atmospheric air is compressed by a four-stage compressor and is stored at 2500 psig in tanks with a combined volume of 141 ft^3. The air is heated by two 420-kW banks of nichrome wire heaters before it enters the tunnel stagnation chamber. The maximum run time is about 60 s.

The tests were conducted at a freestream Mach number of 4.95, a stagnation pressure of 333 psia, and a stagnation temperature of 620°R, corresponding to a freestream Reynolds number of 14.9×10^6 ft^{-1}. The incoming boundary layer underwent natural transition in the nozzle far upstream of the test section and developed under essentially adiabatic wall temperature conditions. Pitot surveys made at the model location showed that the boundary layer was 0.59 in. thick, with displacement and momentum deficit thicknesses of 0.26 and 0.026 in., respectively. The wake strength parameter was 0.78, and the skin friction coefficient was 7.74×10^{-4}.

Models

Five 0.75-in.-thick hemicylindrically blunted fins with leading-edge sweep angles of 0, 8, 18, 30, and 45 deg were used (Fig. 1a). To examine the effects of leading-edge shape, fins with a hemicylindrically blunted leading edge, a 53-deg-half-angle wedge-shaped leading edge (Fig. 1b), and a flat-faced fin (Fig. 1c) were used. The flat-faced fin is not a practical configuration, but was selected because such a strong interaction might provide valuable information on the underlying physics. The hemicylindrical and wedge models were 0.75 in. thick, while the flat-faced model was 0.375 in. The latter thickness was chosen to generate an interaction with the same upstream influence as the wedge and the hemicylindrical models. The height-to-thickness ratio of all fins was greater than 5, and thus each can be considered semi-infinite according to the criterion of Ref. 23.

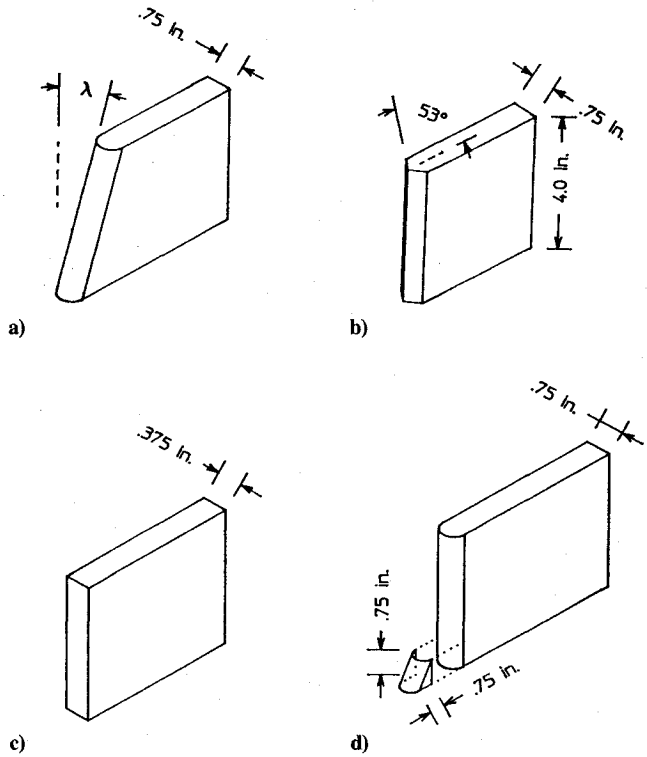

Fig. 1 Model configurations.

Preliminary results from the swept-fin interactions showed significant reductions in upstream influence with increasing λ_{LE}, consistent with earlier work of Refs. 14 and 15. Moreover, the length of the intermittent region (i.e., the region in which the separation shock foot translates) decreased with increasing λ_{LE}. To examine whether the same result could be obtained using a minor modification to the unswept-fin root rather than sweeping the entire fin leading edge, a 45-deg swept fillet was attached to the root of the unswept fin (Fig. 1d). As noted earlier, high-speed schlieren photography reported in Ref. 17 had suggested that this type of fillet reduced unsteadiness, and indeed the preliminary results using the fillet indicated a considerable reduction in the size of the interaction and its unsteadiness.

Instrumentation and Test Procedure

Flush-mounted pressure transducers were used to measure the fluctuating wall pressure. These transducers have a nominal outer diameter of 0.0625 in. and have a frequency response of approximately 50 kHz, due to a protective screen above the 0.028-in.-diam silicon diaphragm. Static calibrations were performed daily using a digital pressure gauge accurate to 0.001 psia. The full-scale output is nominally 75 mV for an applied pressure of 50 psia, resulting in a sensitivity of 1.5 mV/psi. The transducer signals were amplified and low-pass filtered. The filters were normally set at 50 kHz (low-pass mode), but for runs made at 100-kHz sampling frequency, the filters were set at 40 kHz to avoid aliasing. The transducer signals were then digitized by two waveform recorders equipped with 12-bit analog-to-digital converters. In a typical test using eight transducers, 512 records of data per channel with 1024 samples per record were acquired at a sampling rate of 200 kHz/channel.

First, fluctuating wall pressures were measured along the centerline upstream of the fins, using eight transducers at a time. The center-to-center spacing between adjacent transducers was 0.115 in. To improve the spatial resolution, runs were then made with the model shifted by 0.057 in. with the same transducer layout. Second, fluctuating wall pressures were measured simultaneously in the undisturbed flow upstream of the interaction, in the intermittent region, and in the separated region. The second data set was acquired to permit calculations of cross-correlations between transducers upstream and downstream of separation and in the intermittent region in order to determine, if possible, cause and effect.

Analysis Techniques

Statistical analysis included calculations of the mean, standard deviation, skewness, and flatness coefficients and the amplitude probability density distribution. Time-series analysis included cross-correlations and power-spectral-density estimates. Details of such calculation procedures are given in Ref. 24.

Shock Statistics Algorithm

This algorithm converts the intermittent wall pressure-time histories into digital boxcar signals that can be analyzed to quantify the separation shock dynamics.[25] The algorithm distinguishes between the rises and falls in pressure due to the separation shock and those due to turbulent fluctuations in the undisturbed and separated boundary layer.

First the mean pressure of the undisturbed boundary-layer component of the signal and rms of the fluctuations, $\bar{P}_{w0}$ and σ_{pw0}, respectively, are determined. Two thresholds are then defined: $T_1 = \bar{P}_{w0} + 3\sigma_{pw0}$ and $T_2 = \bar{P}_{w0} + 6\sigma_{pw0}$. When the pressure rises above T_2 a rise time t_r, is recorded, and when the pressure then falls below T_1, a fall time t_f, is recorded. For time $t_r < t < t_f$ the boxcar signal is given the value 1, and for all other times it is given the value 0. The shock zero-crossing frequency and the intermittency are then defined by

$$f_c = \frac{1}{(1/N)\sum_{i=1}^{N-1}(t_{r\,i+1} - t_{r\,i})}, \qquad \gamma = \frac{\sum_{i=1}^{N}(t_r - t_f)_i}{t_{\text{total}}} \quad (1)$$

The zero-crossing frequency is the number of unidirectional shock crossings per second over a given location, and the intermittency is the fraction of the total time that the shock is upstream of a particular location.

Separation Shock-Foot Position and Velocity Histories

It is extremely difficult to monitor the separation shock-foot position directly, but it is possible to bracket its location from multichannel wall pressure fluctuations.[26] The binary boxcar signals described above can be nested and the shock-foot position deduced as being either upstream of the entire transducer array, downstream of the array, or between two adjacent transducers. With eight transducers, nine positions (or bins) are possible. The rise and fall times in the boxcar signals identify the coordinates of the instantaneous position of the shock foot, and its position can be estimated at any intermediate time by linear interpolation of these coordinates. The result is a piecewise smooth function for the shock position. The separation shock-velocity history can be calculated knowing the distance between bins and the time taken to pass from one to the other. Further details are given in Ref. 26.

Interaction Length Scales

The distance from the fin leading edge to the separation line was measured directly from surface flow visualization. The intermittent-region length was calculated using a curve fit of the error function, $\gamma = \text{erf}(x)$, to the intermittency curves produced by the shock statistics algorithm. The implicit assumption, borne out by experiments,[27] is that the intermittency is normally distributed between the upstream influence and separation lines. The upstream influence is taken as the distance from the fin leading edge to the location of 1% intermittency, and the intermittent-region length is taken as the distance between points with $\gamma = 5$ and 95%.

Results

Effects of Leading-Edge Sweepback

The mean pressure distributions (Fig. 2) for the hemicylindrically blunted swept fins are consistent with earlier results of Refs. 14 and 15. Increased leading-edge sweep reduces upstream influence, decreases the distance from the leading edge to the initial pressure maximum, and decreases the magnitude of P_M. There is also a substantial decrease in P_{MAX}, the pressure at the fin root (see inset to figure). Over the range $0 < \lambda_{\text{LE}} < 30$ deg, P_{MAX} decreases linearly; beyond this range there appears to be little change.

Distributions of the rms of the pressure fluctuations normalized by freestream static pressure are shown in Fig. 3. The upstream maximum, labeled P_{R1}, is generated by the translating separation shock wave. Initially it does not vary with increasing λ_{LE}, but it decreases for λ_{LE} greater than about 18 deg. This result is not entirely surprising. Until the separated flow is reduced sufficiently in scale to be affected by conditions at the fin root, the separation process itself should remain unchanged. The second maximum, P_{R2}, underneath the separated flow has a similar magnitude to P_{R1} and undergoes the same behavior with increased sweepback. In contrast, the rms at the fin root, P_{R3}, decreases rapidly with increasing sweep, approximately linearly over the range 0–18 deg, and then less rapidly. Loading levels at the root, expressed in decibels and scaled to flight at 50,000 feet, vary from about 186 dB at $\lambda_{\text{LE}} = 0$ deg to about 163 dB at $\lambda_{\text{LE}} = 45$ deg. It should be noted that pressure measurements were made at 0.5ζ (≈ 0.058 in.) upstream of the root. Thus the values of P_{MAX} and P_{R3} are the highest measured values, not necessarily the absolute maxima.

Figures 4a and 4b show the zero-crossing frequency distributions and the variation of the maximum value (which occurs at $\gamma = 50\%$) with leading-edge sweep, while Fig. 4c shows the variation with leading-edge sweep angle of the upstream influence and separation length. It can be seen that $f_{c\,\max}$ increases as the leading-edge sweep angle increases. The weak trend of increasing $f_{c\,\max}$ for increases in λ_{LE} from 8 to 18 deg is much more significant between 18 and 45 deg, and can be explained qualitatively by the reduction in L_i. The intermittent region (i.e., the distance between L_{ui} and L_{sep}) shrinks, but analysis shows that the measured mean and rms shock velocities are constant, regardless of sweep angle. Thus, with a constant shock velocity but a smaller region in which to translate, the shock frequency naturally increases.

Power-spectral-density distributions in the intermittent region at $\gamma \approx 50\%$ are shown in Fig. 5a. As expected, the highest energy levels occur at the lowest frequencies and decrease in intensity with increasing sweepback due to the progressive weakening of the separation shock wave. Normalized spectra in the form G' vs f show that the maximum value of G' occurs close to the maximum shock

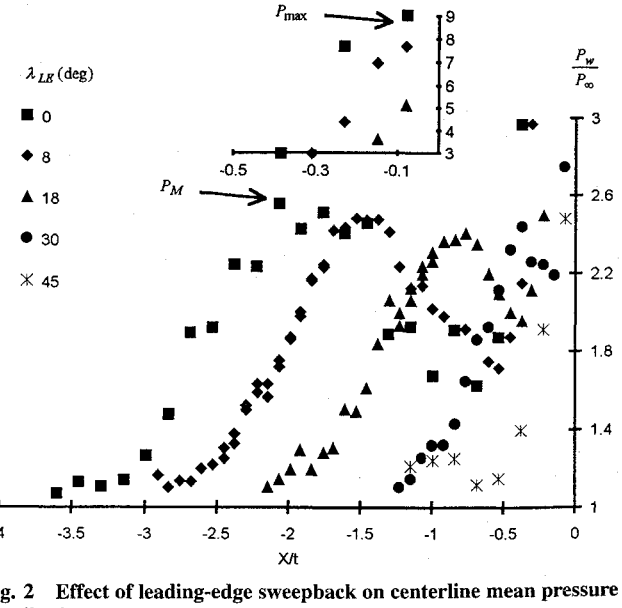

Fig. 2 Effect of leading-edge sweepback on centerline mean pressure distributions.

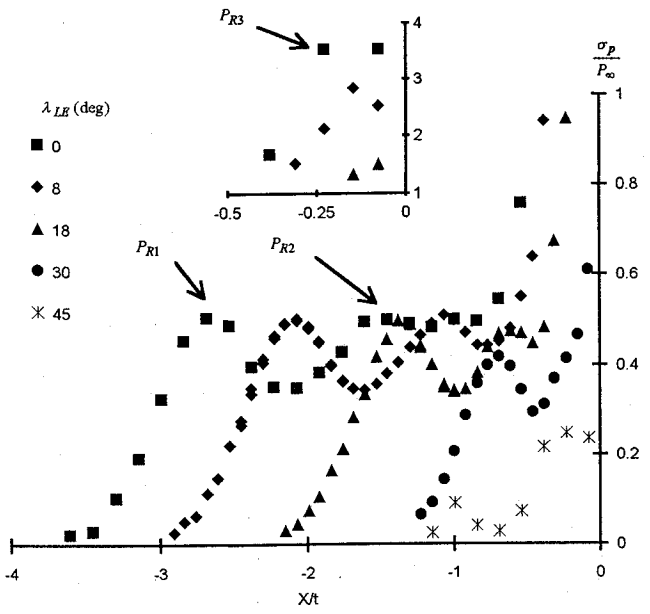

Fig. 3 Effect of leading-edge sweepback on rms of wall pressure fluctuations on centerline.

zero-crossing frequency, demonstrating that pressure fluctuations due to the shock motion dominate the spectral content of pressure signals from the intermittent region.[28] For moderate sweep angles ($0 < \lambda_{LE} < 18$ deg) for which the maximum rms of the pressure fluctuations is the same, there is a slight decrease in low-frequency energy content, which is balanced by a corresponding increase in high-frequency energy content. The 30- and 45-deg cases have a decrease in energy at both low and high frequencies.

Power spectra in the separated region are broadband, and analysis shows that the larger fraction of the variance comes from high frequencies. The effect of increasing sweep is a slight decrease in low-frequency energy content, but, to first order, the spectra are essentially identical. Power spectra of pressure fluctuations at the fin root are shown in Fig. 5b. The large decrease in rms pressure at the fin root is responsible for the decrease in magnitude of the dimensional spectra. The normalized spectra[28] show that, in addition to the reduction in rms, there is some redistribution of energy to higher frequencies; however, to first order, sweep has little effect on the spectral content of the fluctuating wall pressure signals at the fin root.

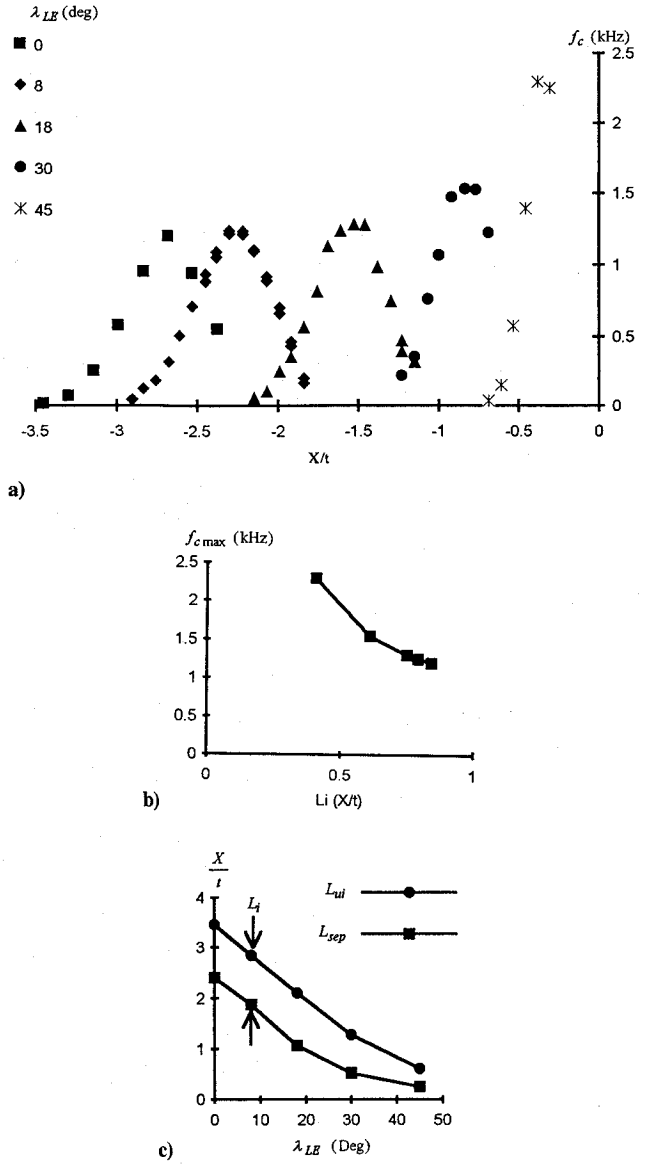

Fig. 4 Effect of leading-edge sweepback on a) shock zero-crossing frequency, b) maximum value, and c) flowfield length scales.

Effects of Leading-Edge Shape

Figures 6 and 7 show distributions of the normalized mean pressure and rms of the pressure fluctuations upstream of the three unswept fins with wedge-shaped, hemicylindrical, and flat-faced leading edges. Since t is different for the flat-faced fin, the x axis is shown unscaled. As intended, the three interactions have approximately the same overall length scale. The magnitudes of P_M and P_{R1} are similar in all three interactions, although the location of these maxima shifts slightly further upstream with increasing fin "bluntness" (i.e., wedge to hemicylindrical to flat-faced). The major differences occur near the fin root; the "blunter" configurations exhibit a marked trough in pressure upstream of the root and, at the root, generate substantially higher mean and rms levels. Even if normalized by the local wall pressure rather than freestream static pressure, the rms near the fin root is still larger for the blunter configurations. The flowfield structural changes responsible for these phenomena are discussed later.

The intermittent region lengths for the hemicylindrical, wedge, and flat leading edges are 0.6, 0.83, and 0.49 in., respectively, which correspond to $0.8t$, $1.1t$, and $1.3t$, respectively. The normalized value for the hemicylindrical case is consistent with correlations presented in Ref. 29. During the current study, a thicker flat fin ($t = 0.5$ in.) was also tested, and it too had $L_i = 1.3t$; thus, this value seems consistent. So, in terms of fin thickness, the intermittent region is about 60% larger for the flat model than for the hemicylindrical model. The maximum separation shock zero-crossing frequency increases from 0.8 to 1.5 kHz as the leading edge changes from wedge-shaped to hemicylindrical to flat. However, as with sweepback, this effect is not due to any fundamental change in shock dynamics, expressed in terms of mean shock velocity or shock-velocity fluctuations. Reemphasizing what was said earlier, f_C increases because a shock wave with constant mean and rms velocity is constrained to move within a smaller region. Thus a key question is why a change in leading-edge shape generates interactions with the same overall length scale but with different intermittent-region length scales. Put differently, what flowfield structural changes are induced by the leading-edge shape change, and why do these alter the length scale of the shock-wave motion? This question is addressed later, following some brief remarks about the power spectra and some comments on the effects of leading-edge modifications.

Power spectra from the intermittent region are shown in Fig. 8. As might be anticipated from the similarities in the shapes and magnitudes of the mean and rms pressures near separation (Figs. 6 and 7), the spectra are very similar. Similarly, spectra from the separated region are almost indistinguishable. At the fin root there are large variations in maximum rms with change in shape, but there is little difference in the relative distribution of the variance across the frequency domain (Fig. 8), only a decrease in absolute level with decreasing bluntness.

Leading-Edge Modifications

The 45-deg fillet had a profound effect on the flowfield upstream of the unswept hemicylindrically blunted fin. Figures 9a and 9b show the centerline normalized mean pressure and rms of the pressure fluctuations with and without the modification. Also shown are results for the 45-deg swept fin. The distributions upstream of the 45-deg swept fin and the unswept fin with a 45-deg fillet are identical. Compared to the unswept case without a fillet, the upstream influence and the intermittent region lengths are reduced by 50%. The mean and rms loading levels at the fin root are reduced by about 75% and 95%, respectively. The use of a swept fillet at the fin root appears to be an excellent way to obtain the benefits of leading-edge sweep without sacrificing the surface area of acontrol.

Discussion

Although a complete explanation of how the flowfield structure and subsequent fluctuating loads are affected by leading-edge sweepback and shape change is lacking, the results described in this section provide some new insights into the processes involved. That the separation shock motion is influenced by fluctuations in the incoming boundary layer is evident from cross-correlations of separation shock-velocity fluctuations with wall pressure fluctuations under the undisturbed boundary layer. Results for $\lambda_{LE} = 8$ and 30 deg are shown in Fig. 10. The maximum cross-correlation coefficient is at negative τ, showing that pressure fluctuations in the boundary layer precede shock-velocity fluctuations. Peak P_1 occurs at -40 μs for $\lambda_{LE} = 8$ deg and at -25 μs for $\lambda_{LE} = 30$ deg, and is the time delay required for the fluctuation to be convected from

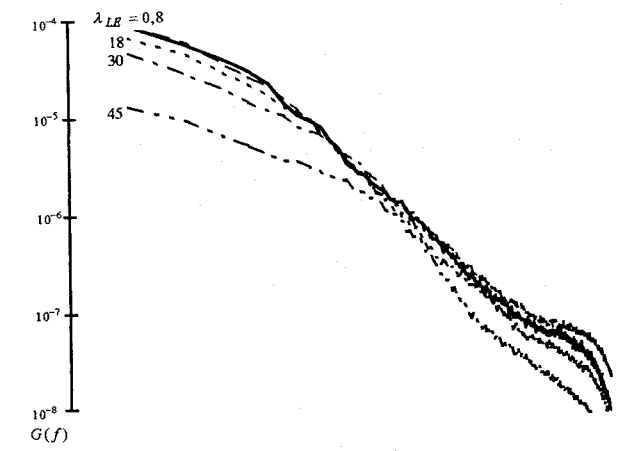

a)

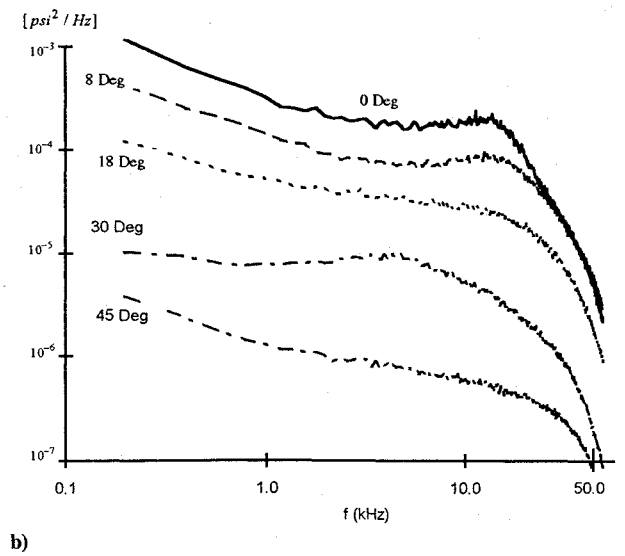

b)

Fig. 5 Effect of leading-edge sweepback on power spectral density in a) intermittent region at $\gamma = 50\%$ and b) root region.

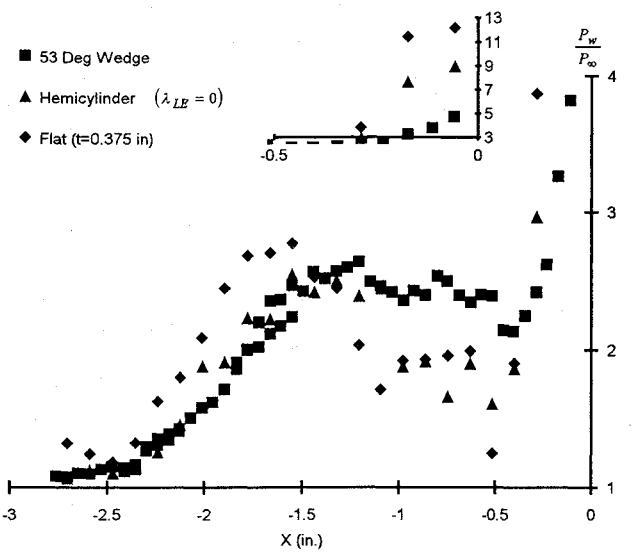

Fig. 6 Effect of leading-edge shape on centerline mean pressure distribution.

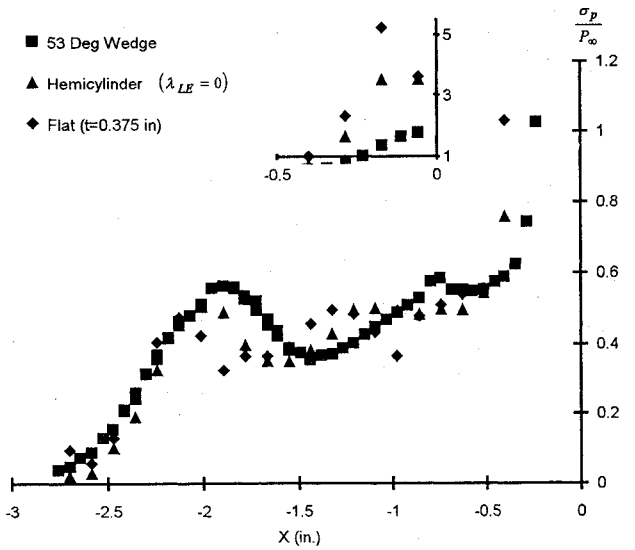

Fig. 7 Effect of leading-edge shape on the rms of the pressure fluctuations on the centerline.

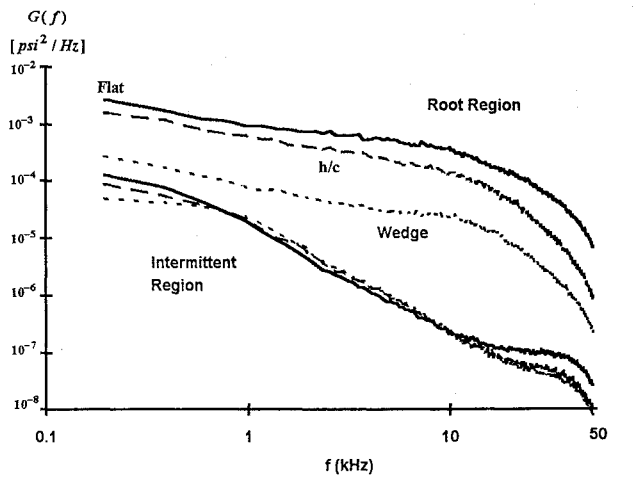

Fig. 8 Effect of leading-edge shape on power spectral density in the intermittent region at $\gamma = 50\%$ and at the fin root.

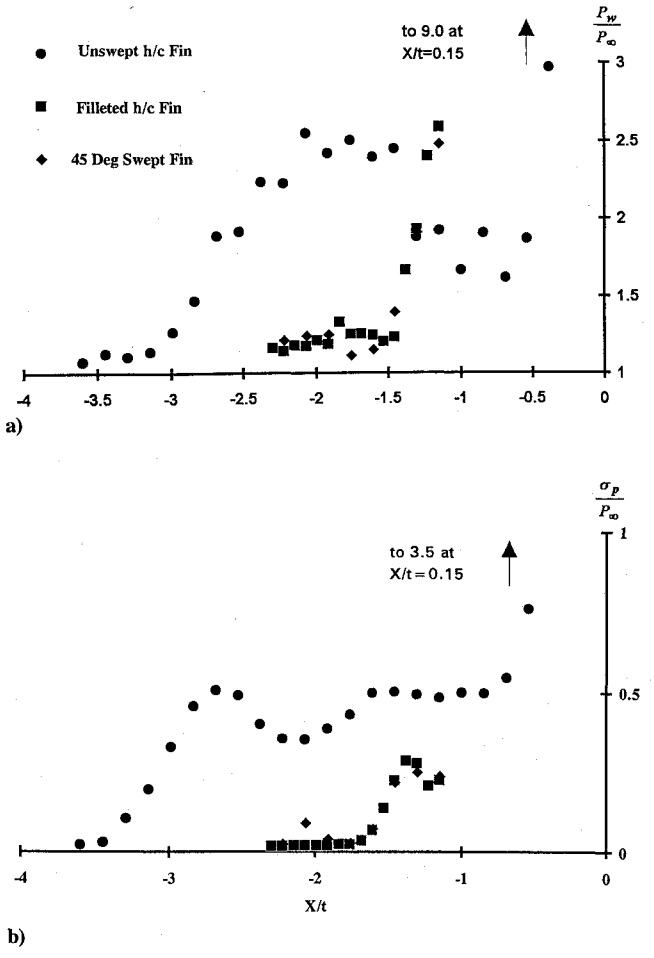

Fig. 9 Effect of root fillet on a) centerline mean wall pressure distribution and b) rms of pressure fluctuations on centerline.

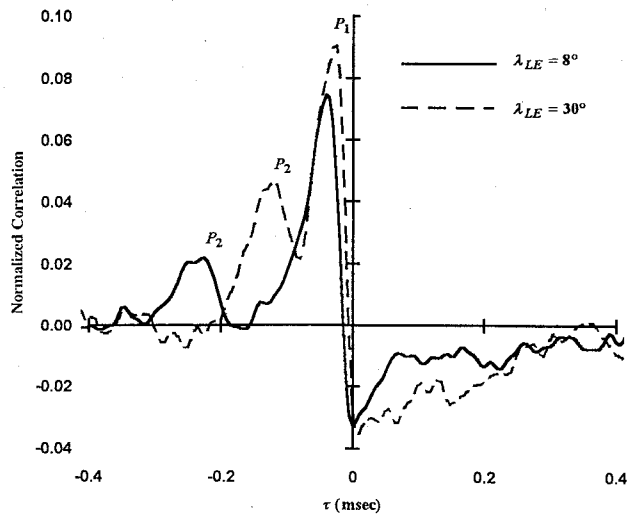

Fig. 10 Cross-correlations of shock-velocity fluctuations with wall pressure fluctuations under the undisturbed boundary layer.

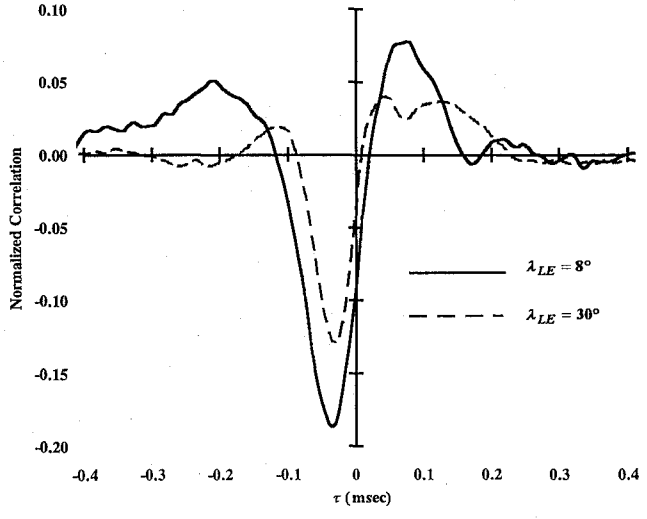

Fig. 11 Cross-correlations of shock-velocity fluctuations with wall pressure fluctuations under the separated flow.

the upstream transducer to the downstream station at which shock-velocity fluctuations occur. Since the velocity history is deduced from several transducers spanning the intermittent region, the location of the downstream station is effectively the middle of the intermittent region. The intermittent region is shorter in the more highly swept case (Fig. 4); thus P_1 occurs at the shorter time. Based on these time delays and on the physical separation distances, a convection velocity of 60–70% U_∞ is obtained in both cases.

Figure 10 also shows that recirculating turbulent structures influence the shock motion. In both correlations, secondary peaks occur which are smaller in magnitude than P_1 and are at larger negative time delays. Physically, a turbulent structure passes through the separation shock, then through the separated shear layer to the fin root region, and is recirculated upstream, again influencing the shock motion. Not all structures entering the interaction are recirculated upstream to the shock foot, and not all structures remain coherent over such a distance; thus $P_1 > P_2$. Since the upstream influence for $\lambda_{LE} = 8$ deg is much larger than for $\lambda_{LE} = 30$ deg, the time required to travel to the fin root and then upstream to the intermittent region is larger for the former than for the latter; hence, a larger time delay for P_2 in the less-swept case. Moreover, the magnitude of P_2 for $\lambda_{LE} = 8$ deg is smaller than for $\lambda_{LE} = 30$ deg, because the physical distance is larger and structures are less likely to remain coherent and be recirculated as far upstream as the intermittent region. For interactions with the same upstream influence (i.e., flat-faced and wedge-shaped leading edges), P_2 occurs at about the same time delay,[28] providing strong support for the argument made earlier.

Cross-correlations of the shock-velocity fluctuations with pressure fluctuations under the separated flow are shown in Fig. 11 for $\lambda_{LE} = 8$ and 30 deg. The maximum cross-correlation coefficient, indicated by P_1, is at negative time delay, showing that separated flow fluctuations precede shock velocity fluctuations. The magnitude of the time delay is smaller for $\lambda_{LE} = 30$ deg, because the distance from the transducer to the intermittent region is smaller. Reference 11 obtained similar cross-correlations in swept and unswept compression ramp flows, as well as in blunt-fin flows, and has shown that the main cause of the shock motion is its displacement due to the relatively low-frequency expansion and contraction of the separated flow. A key question with respect to control is therefore how the structure and dynamics of the separated flow are influenced by sweep and leading-edge shape.

Considering shape first, Fig. 12 shows the measured mean wall pressure and skewness coefficient distribution upstream of the flat-faced fin. Also shown is the wall pressure measured by Ref. 18 using the same model geometry but with $t = 0.25$ in. The freestream conditions are the same, but the boundary layer is thinner ($\delta \approx 0.2$ in.). The two experiments agree well, confirming that the interaction scale and pressure distribution shape are controlled primarily by t. Moreover, the minor differences between the two sets of measurements suggest that the same flow structure exists in both experiments. Also shown in Fig. 12 is the wall pressure distribution computed by Hung[22] for the incoming flow conditions and geometry used in Ref. 18. The computations exhibit the same features as the measurements, suggesting that they capture the essential flowfield structure. Figure 12 shows the computed particle paths on the plane of symmetry, showing the bifurcated vortex structure. According to Ref. 22, there are two maxima in the upstream u component of velocity under the cores of the two vortices. Between the two maxima,

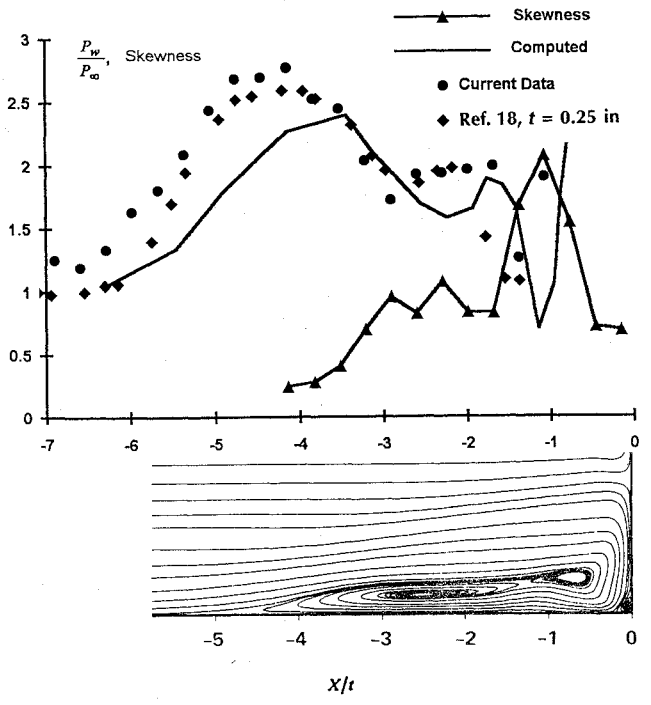

Fig. 12 Flat-faced fin: Measured and computed mean wall pressure distribution, skewness distribution, and particle paths computed by Hung.[22]

the reverse velocity slows down and then accelerates, leading to the kink in the wall pressure around $x/t = -1.5$. Note that the local peak in skewness coefficient coincides with the drop in pressure and also to the position of the vortex boundaries.

Computations are not available for the wedge-shaped leading edge, but the wall pressure and skewness distribution (Fig. 13) suggest that the flow structure is probably qualitatively similar to that of the flat fin. The pressure drop just upstream of the root is smaller, suggesting that the secondary vortex is much weaker, inducing less reverse-flow acceleration. Further, the location of the pressure drop and the skewness coefficient peak are closer to the fin, indicative of a smaller secondary vortex. Computations are also not available for the hemicylindrical leading edge at Mach 5, although Ref. 19 computed this case at Mach 3. The computed pressure distribution and the Mach 3 experimental data of Ref. 20 are shown in Fig. 14. The current pressure distribution at Mach 5 is also shown and has the same shape as at Mach 3, although the pressure magnitudes are larger on account of the stronger shocks. Neither the measurements nor the computations display the pressure kink seen with the flat-faced fins, and the computed particle paths (Fig. 14) show only a single vortex (other than the tiny root vortex, which occurs with all geometries).

How these changes in flow structure alter the unsteadiness and loading levels is not entirely clear. For the flat model σ_p rises rapidly about $1t$ upstream of the leading edge, while for the hemicylindrical model the rise occurs at about $0.4t$. The former location (Fig. 12) corresponds to the leading edge of the secondary vortex, while the latter corresponds to the downstream end of the primary vortex. It is probable that the expansion-contraction process of the vortex causes large local pressure variations at its boundaries, resulting in the increase in rms at these stations. The location of the maximum rms close to the root is not well resolved, but is in the vicinity of $x/t = -0.5$ and $-0.15t$ for the flat and hemicylindrical models. In this region of very high mean pressure gradients, expansion and contraction of the vortex subjects a fixed station on the test surface to large pressure variations, generating large rms values. As might be expected intuitively and is confirmed by computation,[21] as the primary vortex is weakened and reduced in scale through increasing leading-edge sweepback, the maximum rms decreases and moves closer to the leading edge.

Since the overall flowfield length scale is to a first approximation given by kt (where k, a constant, depends on leading-edge shape),

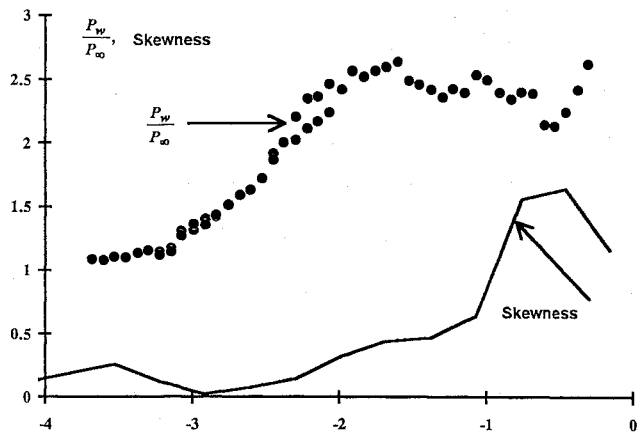

Fig. 13 Mean wall pressure and skewness distributions upstream of fin with wedge-shaped leading edge.

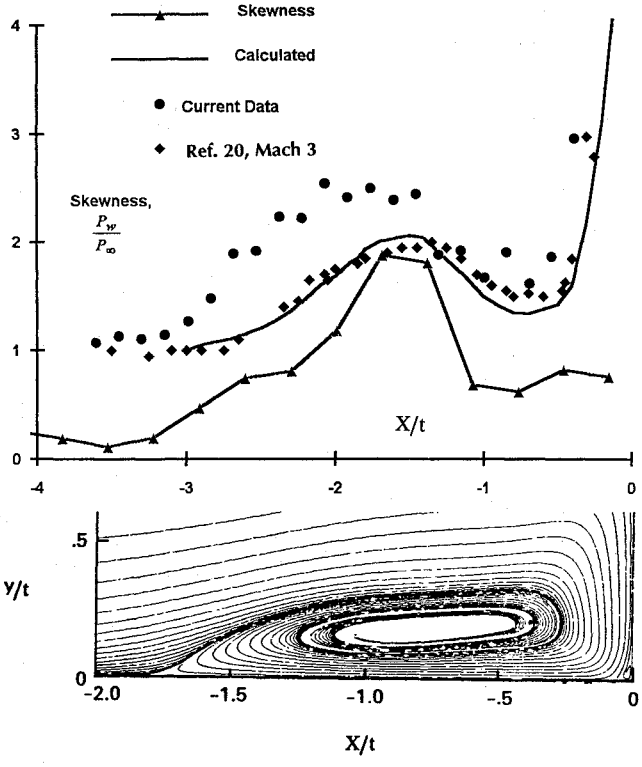

Fig. 14 Hemicylindrical fin: Measured and computed mean wall pressure distribution, skewness distribution, and particle paths computed by Hung and Buning.[19]

it is reasonable to assume that the primary vortex will also scale on t. If the primary vortex expands and contracts the same amount relative to its mean scale, then it is possible that the intermittent-region length also scales on primary vortex size. This is certainly the case if experiments are conducted in a given boundary layer using unswept hemicylindrically blunted fins of different diameter. In that case, the overall flowfield scale and primary vortex size increase with D, but L_i remains fixed at about $0.8D$. However, without detailed flow structure information, it is difficult to estimate how the primary vortex length scale changes with leading-edge geometry; so this argument is difficult to substantiate. Since the upstream edge of the primary vortex varies between the upstream influence and separation lines, the mean upstream edge can, as an approximation, be taken as being at $\gamma = 50\%$. In the hemicylindrical case, the computations suggest that the downstream edge is at the fin leading edge, whereas for the flat case it is at the pressure minimum (Fig. 12) near $x/t = -1.4$ (i.e., at the bifurcation point of the primary and secondary vortices). Both cases generate a ratio of intermittent region length to mean vortex length of about 0.3. On the other hand, with the

wedge, the ratio is about 0.5 if the downstream end is taken at the pressure minimum and 0.38 if taken at the fin leading edge.

Conclusions

Measurements of the fluctuating wall pressure have been made on centerline upstream of blunt fins in a Mach 5 turbulent boundary layer to examine the effects of leading-edge sweepback, leading-edge shape, and fin root modifications on the fluctuating loads. The results show the following:

1) There are practical benefits to be obtained from leading-edge sweep. Although the mean and rms loading levels in the intermittent region are unaffected by moderate sweepback, the mean and rms pressure at the fin root are reduced by about 40 and 60%, respectively, with 18 deg of leading-edge sweep. This reduction in root loading is coupled with a significant reduction of the interaction length scale (by about 80% in the 45-deg swept case). Leading-edge sweep has little effect on the spectral content of the pressure fluctuations in the separated region, but the spectral content of fluctuations in the intermittent region shifts to higher frequencies for greater sweep angles.

2) A 45-deg swept hemicylindrically blunted root fillet reduces the centerline upstream influence and intermittent-region length by 50% and reduces the mean and rms pressure loading at the fin root by about 75 and 95%, respectively.

3) Fin leading-edge shape affects the structure of the separated flowfield, which in turn alters the flowfield unsteadiness. Experiments using hemicylindrical, 53-deg wedge, and flat leading edges show that root loading increases with increasing bluntness (i.e., wedge to hemicylinder to flat), and intermittent-region length (in terms of fin thicknesses) also increases with increased bluntness.

4) Cross-correlations of separation shock-velocity fluctuations with pressure fluctuations in the incoming boundary layer and under the separated flow show that fluctuations in both regions correlate with and precede the shock motion. Current and previous experiments show that the expansion and contraction of the separated flow dominates the process. The physical extent of the expansion-contraction process appears to depend on the details of the flowfield structure, not on its overall size. Recirculation of large-scale turbulent structures also plays a role in influencing the shock motion, and the recirculation process depends on the type and scale of the separated flow.

Acknowledgments

This work was supported by NASA Langley under Grant NAG1-1005, monitored by W. E. Zorumski. Financial support for the graduate studies of the first author was provided by the United States Air Force. These sources of support are gratefully acknowledged. Special thanks also go to Mehmet Erengil, Leon Brusniak, Edward Zihlman Jr., and Frank Wise for advice and assistance with hardware and software.

References

[1]Robertson, J. E., "Characteristics of the Static and Fluctuating-Pressure Environments Induced by Three-Dimensional Protuberances at Transonic Mach Numbers," Wyle Lab., WR-69-3, 1969.

[2]Robertson, J. E., "Prediction of In-Flight Fluctuating-Pressure Environments Including Protuberance Induced Flow," Wyle Lab., WR-71-10, 1971.

[3]Dolling, D. S., and Bogdonoff, S. M., "An Experimental Investigation of the Unsteady Behavior of Blunt Fin-Induced Shock Wave Turbulent Boundary Layer Interactions," AIAA Paper 81-1287, June 1981.

[4]Aso, S., Kuranaga, S., and Hayashi, M., "Detailed Measurements on Unsteady Properties in Three Dimensional Shock Wave/Turbulent Boundary Layer Interaction Induced by Blunt Fin at Mach Number 4," AIAA Paper 91-1755, June 1991.

[5]Dolling, D. S., and Smith, D. R., "Unsteady Shock-Induced Separation in Mach 5 Cylinder Interactions," *AIAA Journal*, Vol. 27, No. 12, 1989, pp. 1098–1706.

[6]Shifen, W., and Qingquan, L., "Hypersonic Turbulent Separated Flow Past an Unswept Circular Cylinder on a Flat Plate," *Acta Aerodynamica Sinica*, Vol. 10, No. 1, 1992, pp. 38–44.

[7]Gramann, R. A., and Dolling, D. S., "Interpretation of Separation Lines from Surface Tracers in a Shock-Induced Turbulent Flow," *AIAA Journal*, Vol. 25, No. 12, 1987, pp. 1545,1546.

[8]Dolling, D. S., "Fluctuating Loads in Shock Wave/Turbulent Boundary Layer Interactions: Tutorial and Update," AIAA Paper 93-0284, Jan. 1993.

[9]Gramann, R. A., and Dolling, D. S., "Detection of Turbulent Boundary Layer Separation Using Fluctuating Wall Pressure Signals," *AIAA Journal*, Vol. 28, No. 6, 1990, pp. 1052–1056.

[10]Pozefsky, P., Blevins, R. D., and Laganelli, A. L., "Thermo-Vibro-Acoustic Loads and Fatigue of Hypersonic Flight Vehicle Structures," AFWAL TR-89-3-14, Feb. 1989.

[11]Erengil, M. E., and Dolling, D. S., "Physical Causes of Separation Shock Unsteadiness in Shock Wave Turbulent Boundary Layer Interactions," AIAA Paper 93-3134, July 1993.

[12]Dolling, D. S., and Brusniak, L., "Correlation of Separation Shock Motion in a Cylinder-Induced Interaction with Pressure Fluctuations under the Separated Region," AIAA Paper 91-0650, Jan. 1991.

[13]Brusniak, L., and Dolling, D. S., "Flowfield Dynamics in Blunt Fin-Induced Shock Wave Turbulent Boundary Layer Interaction," AIAA Paper 93-3133, July 1993.

[14]Price, E. A., and Stallings, R. L., "Investigation of Turbulent Separated Flows in the Vicinity of Fin-Type Protuberances at Supersonic Mach Numbers," NASA TN D-3804, 1967.

[15]Hussain, S., "A Study of the Interaction Between a Glancing Shock Wave and a Turbulent Boundary Layer—The Effects of Leading Edge Bluntness and Sweep," Ph.D. Thesis, College of Aeronautics, Cranfield Inst. of Technology, Nov. 1985.

[16]Sedney, R., "A Survey of the Effects of Small Protuberances on Boundary Layer Flows," *AIAA Journal*, Vol. 11, No. 6, pp. 782–792.

[17]Blank, S. C., "The Effect of Junction Modifications on Glancing Interaction—Blunt Fins," private communication, Jan. 1993.

[18]Dolling, D. S., and Rodi, P. E., "Upstream Influence and Separation Scales in Fin-Induced Shock Turbulent Boundary Layer Interaction," *Journal of Spacecraft and Rockets*, Vol. 25, No. 2, 1988, pp. 102–108.

[19]Hung, C.-M., and Buning, P. G., "Simulation of Blunt Fin Induced Shock Waves and Turbulent Boundary Layer Interaction," *Journal of Fluid Mechanics*, Vol. 154, May 1985, pp. 163–185.

[20]Dolling, D. S., and Bogdonoff, S. M., "Blunt Fin-Induced Shock Wave Turbulent Boundary Layer Interaction," *AIAA Journal*, Vol. 20, No. 12, 1982, pp. 1674–1680.

[21]Lakshmanan, B., and Tiwari, S. N., "Study of Supersonic Intersection Flowfield at Modified Wing-Body Junctions," *AIAA Journal*, Vol. 31, No. 5, 1993, pp. 877–883.

[22]Hung, C.-M., "Computation of Navier-Stokes Equations for Three Dimensional Flow Separation," NASA TM 102266, Dec. 1989.

[23]Dolling, D. S., and Bogdonoff, S. M., "Scaling of Interactions of Cylinders with Supersonic Turbulent Boundary Layers," *AIAA Journal*, Vol. 19, No. 5, 1981, pp. 655–657.

[24]Bendat, J. S., and Piersol, A. G., *Random Data, Analysis and Measurement Procedures*, 2nd Ed., Wiley, New York, 1986.

[25]Brusniak, L., "Evaluation of Conditional Sampling Methods of Analyzing Separation Shock Motion," AIAA Paper 88-0091, Jan. 1988.

[26]Erengil, M. E., and Dolling, D. S., "Effects of Sweepback on Unsteady Separation in Mach 5 Compression Ramp Interactions," *AIAA Journal*, Vol. 31, No. 2, 1993, pp. 302–311.

[27]Erengil, M. E., and Dolling, D. S., "Correlation of Separation Shock Motion with Pressure Fluctuations in the Incoming Boundary Layer," *AIAA Journal*, Vol. 29, No. 11, 1991, pp. 1868–1877.

[28]Kleifges, K., and Dolling, D. S., "Control of Unsteady Shock-Induced Turbulent Boundary Layer Separation Upstream of Blunt Fins," AIAA Paper 93-3281, July 1993.

[29]Gonsalez, J. C., and Dolling, D. S., "Correlation of Interaction Sweepback Effects on the Dynamics of Shock-Induced Turbulent Separation," AIAA Paper 93-0776, Jan. 1993.

J. M. Allen
Associate Editor